Polyhedron 123 (2017) 122–131

Contents lists available at ScienceDirect

Polyhedron

journal homepage: www.elsevier.com/locate/poly

Low spin Fe(II) complexes formed of monosubstitued 2,6-bis(2-benzimidazolyl)pyridine ligands

Cyril Rajnák [a,b,c,*], Ján Titiš [a], Olaf Fuhr [b,d], Mario Ruben [b,c], Roman Boča [a]

[a] Department of Chemistry, FPV, University of SS Cyril and Methodius, 91701 Trnava, Slovakia
[b] Institute of Nanotechnology, Karlsruhe Institute of Technology (KIT), 76021 Karlsruhe, Germany
[c] IPCMS-CNRS, Université de Strasbourg, 23, rue du Loess, f-67034 Strasbourg, France
[d] Karlsruhe Nano-Micro Facility (KNMF), Karlsruhe Institute of Technology (KIT), 76021 Karlsruhe, Germany

ARTICLE INFO

Article history:
Received 28 July 2016
Accepted 5 November 2016
Available online 17 November 2016

Keywords:
Crystal structure
Derivates of 2,6-bis(2-benzimidazolyl) pyridine
Fe(II) complex
Magnetic data
Low spin complexes

ABSTRACT

Five ligands as monosubstituted derivatives of the basic skeleton of 2,6-bis(2-benzimidazyl)pyridine were synthesized, and characterized by NMR and IR spectra along with the X-ray structure analysis. Their complexation gave a set of hexacoordinate Fe(II) complexes showing predominantly the diamagnetism until ambient temperature. Some temperature-independent paramagnetism along with an onset of the spin transition is also detected.

1. Introduction

The condensation product of the *o*-phenylenediamine with pyridine-2,6-dicarboxylic acid results in the formation of 2,6-bis (2-benzimidazolyl)pyridine, abbr. *bzimpy*. The *bzimpy* ligand became one of the most useful starting materials for more complicated organic compounds e.g. anchoring and ancillary ligands used to coordination chemistry [1–3]. The benzimidazole group is also known as a good provider of greater coordination bonding due to strong σ donor effect [4]. This ligand has been widely combined with metal ions yielding a number of transition metal complexes that were studied from various aspects in detail [5]. The high and low spin Fe(II) complexes with six-membered ring ligands were studied largely [6–13]. One target of investigation was oriented to magnetic studies as Fe(II) complexes of the formula $[Fe(bzimpy)_2]X_2{\cdot}sol$ are susceptible for spin crossover from the low-spin state $S = 0$ to the high-spin state $S = 2$ [14–16]; X – monoanion, *sol* – crystal solvent. Also deprotonation of the basic ligand *bzimpy* to $bzimpy_{-1H}$ gave neutral Fe(II) complex with interesting magnetic behaviour [17].

Herein we are reporting about synthesis and characterization of new ligands L^2 through L^6 as derivatives of the basic ligand L^1 = *bzimpy* (Scheme 1). Their complexation with Fe(II) salts produced a set of hexacoordinate complexes $[Fe(L^n)_2](ClO_4)_2$ and $[Fe(L^n{}_{-1H})_2]$ whose magnetic properties, after structure determination, were studied in detail (Scheme 2).

2. Experimental

2.1. Chemicals and handling

All chemicals of reagent grade quality were purchased and used as received (Sigma–Aldrich, Merck). The solvents dichloromethane, methanol for column chromatography were used without further purification. Other solvents, acetonitrile, *N*,*N*-dimethylformamide and toluene were distilled with dehydrating agent CaH_2 under inert argon atmosphere. Dichloromethane for synthesis was purified analogously. ^1H and ^{13}C NMR measurements of ligands were conducted in DMSO-d_6.

CAUTION. Handling with metal–organic perchlorates is potentially dangerous due to their explosive properties. It should be handled with care in small quantities. Especially high-temperature magnetic measurements are risky.

2.2. Physical measurements

Elemental analysis was carried out by the vario MICRO cube analyzer (Elementar Analysensysteme) and Flash 2000 CHNS/O

* Corresponding author at: Department of Chemistry, FPV, University of SS Cyril and Methodius, 91701 Trnava, Slovakia.
E-mail address: cyril.rajnak@ucm.sk (C. Rajnák).

http://dx.doi.org/10.1016/j.poly.2016.11.009
0277-5387/

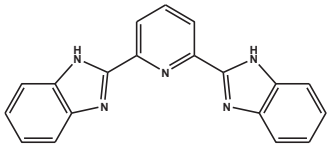

L^1, *bzimpy,*
2,6-bis(2-benzimidazolyl)pyridine

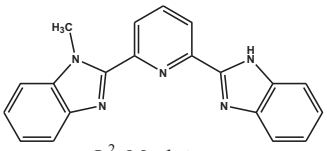

L^2, Me-*bzimpy*,
2-[6-(1H-benzimidazol-2-yl)-pyridin-2-yl]-1-methyl-1H-benzimidazole

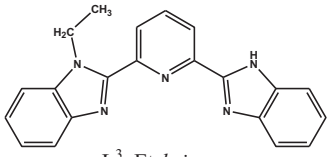

L^3, Et-*bzimpy,*
2-[6-(1H-benzimidazol-2-yl)-pyridin-2-yl]-1-ethyl-1H-benzoimidazole

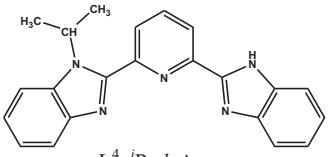

L^4, ^{i}Pr-*bzimpy,*
2-[6-(1H-benzimidazol-2-yl)-pyridin-2-yl]-1-*iso*propyl-1H-benzimidazole

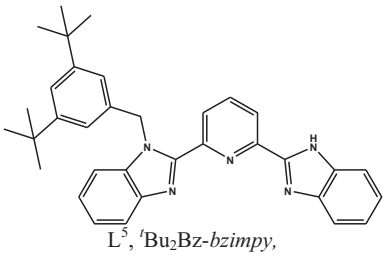

L^5, $^{t}Bu_2$Bz-*bzimpy,*
2-[6-(1H-benzimidazol-2-yl)-pyridin-2-yl]-1-(3,5-di-*tert*-butyl-benzyl)-1H-benzoimidazole

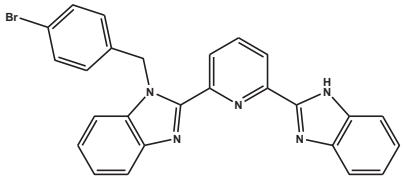

L^6, BrBz-*bzimpy,*
2-[6-(1H-benzimidazol-2-yl)-pyridin-2-yl]-1-(4-bromo-benzyl)-1H-benzimidazole

Scheme 1. Sketch of the ligands L^1 through L^6.

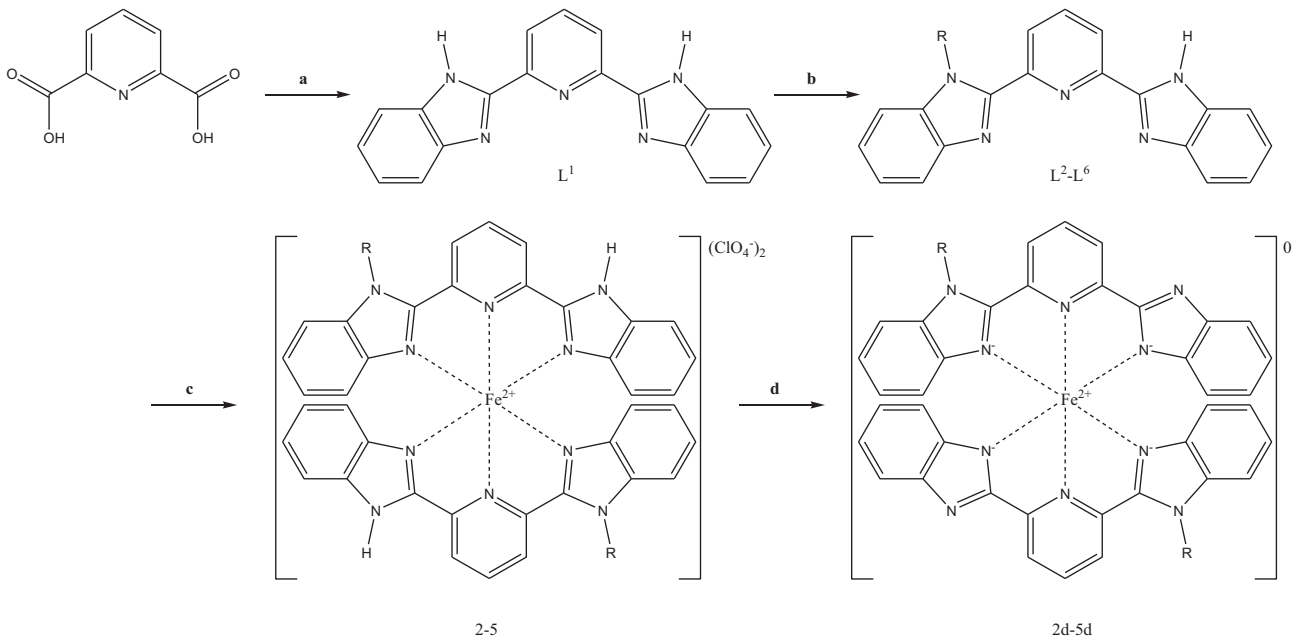

Scheme 2. Synthetic path: (a) phosphoric acid (200 °C), *o*-phenylenediamine, (b) NaH, SA c) CH_3OH, $Fe(H_2O)_6(ClO_4)_2$, Ar, 60 °C, (d) Na_2CO_3, CH_2Cl_2, Ar, 39 °C.

apparatus (Thermo Scientific). The NMR spectra of ligands were measured using FT-NMR Spectrometer (Avance III 500, Bruker) and analyzed by TOPSPIN 1.2. Prior to using, the solid KBr for FT-IR measurements was kept against absorption of moisture in an oven at 60 °C. FT-IR spectra were measured in KBr pellets (Spectrum GX, Perkin Elmer). Absorption UV-Vis spectra were recorded by two-beam UV–Vis-NIR spectrophotometer (Cary 500 Scan). Electrospray ionization time of flight (ESI-TOF) mass spectrometry was acquired on a micrOTOF-Q II (Bruker) spectrometer in the positive mode of ion polarity. Melting points were studied with thermo-microscopy via a Kofler hot-stage microscope at 4 °C min^{-1} and reported without corrections.

2.2. Synthesis of 2,6-bis(2-benzimidazolyl)pyridine (L^1)

Pyridine-2,6-dicarboxylic acid (6.68 g, 40 mmol) was stirred with *o*-phenylenediamine (9.52 g, 88 mmol) in syrupy 85% phosphoric acid (60–70 cm^3) at 220 °C for overnight [18,19]. The blue coloured melt was poured into 1000 cm^3 of vigorously stirred cold water for 1 h. The blue precipitate was collected by filtration through a Büchner funnel, then slurried in 1000 cm^3 of 10% aqueous sodium carbonate for 1 h to obtain ochroid-pink colour. The resulting solid was filtered off and recrystallized from hot methanol solution (250 cm^3) and activated charcoal to give long, white needles. Yield: 5.70 g, 46%. Melting point 353–355 °C. ESI-TOF MS (CH_2Cl_2): m/z = 334.11 M + Na^+. ^{1}H NMR (500 MHz, DMSO-d_6, 25 °C) δ(ppm) 12.99 (s, 2H), 8.33 (d, J = 7.5, 2H), 8.17 (t, J = 7.5 Hz, 1H), 7.75 (t, J = 4.5, 4H), 7.31 (q, J = 2.5, 4H). ^{13}C NMR (125 MHz, DMSO-d_6, 25 °C) δ(ppm) 150.47, 147.73, 139.19, 123.04, 121.35, 79.14. FT-IR (KBr): ν/cm^{-1} = 3178, 3061, 1775, 1623, 1601(m), 1591, 1573(m), 1491, 1459(s), 1436(s), 1383, 1320(s), 1277(s), 1230, 1146, 1115, 1102, 1023, 1013, 995, 963, 929, 902, 880, 845, 822, 803, 767, 742(s), 693, 655, 622, 570, 557. Elemental analysis calc. $C_{19}H_{13}N_5$: C, 73.3; H, 4.21; N, 22.5. Found: C, 73.0; H, 4.45; N, 22.2%. X-ray structure analysis: $C_{19}H_{13}N_5{\cdot}3CH_3OH$, M = 407.47 g mol^{-1}.

2.4. Synthesis of ligands L^2 through L^6

Monosubstituted ligands based upon the *bzimpy* skeleton have been synthesized by a general recipe as follows. The substituting agent (SA) was MeI, EtI, ^{i}PrI, 3,5-di-(*tert*-butyl)-benzyl bromide, and 4-bromobenzyl bromide for L^2 through L^6, respectively [20].

N,*N*-dimethylformamide was distilled with dehydrating agent CaH_2 under inert argon atmosphere. A 250 cm^3 three necked flask was charged with *bzimpy* (2.30 g, 7.38 mmol) and 100 cm^3 of freshly distilled dimethylformamide and then degassed. NaH (dispersion 60%, 0.29 g, 7.38 mmol) was suspended in 10 cm^3 of dry dimethylformamide under an inert atmosphere and then added drop-by-drop to the basic solution cooled down at *ca* 0 °C under argon. The mixture was allowed to stand at room temperature for 1 h. The mixture was cooled again to 0 °C, SA (5.54 mmol) was added dropwise and the mixture was heated to 40 °C for overnight. The purification by column chromatography was carried out on Al_2O_3 dichlomethane and methanol (150:1). The crude product was recrystallized from appropriate solvent (30 cm^3). A single crystal of good quality was used for the X-ray diffraction studies.

Data for L^2. Yield: 0.53 g, 22%, white powder. Melting point: 241–243 °C. Thin layer chromatography (CH_2Cl_2/CH_3OH; 150:1): R_f ~0.48. ESI-TOF MS (CH_2Cl_2): m/z = 348.13, (theoretical m/z = 348.12 M + Na^+. ^{1}H NMR (500 MHz, DMSO-d_6, 25 °C) δ (ppm) 12.79 (s, 1H), 8.44 (dd, J = 7.75, 1H), 8.32 (dd, J = 7.75 Hz, 1H), 8.18 (t, J = 7.75, 1H), 7.76 (dd, J = 8, 2H), 7.69 (s, 2H), 7.37 (t, J = 7.75, 1H), 7.32–7.26 (m, 3H), 4.33 (s, 3H). ^{13}C NMR (125 MHz, DMSO-d_6, 25 °C) δ(ppm) 149.03, 148.69, 148.63, 146.76, 140.93, 137.54, 135.91, 124.12, 122.16, 121.27, 120.72, 118.39, 116.94, 109.69, 31.59. FT-IR (KBr): ν/cm^{-1} = 3392, 3057, 2946, 1932, 1891, 1769, 1594(m), 1572(m), 1468, 1435(s), 1396, 1380, 1315, 1276, 1262, 1230, 1155, 1072, 1006, 994, 972, 928, 903, 856, 824 (m), 742(s), 658, 618, 588, 565, 455, 426. UV/VIS (CH_2Cl_2): λ_{max} (ε, M^{-1} cm^{-1}) = 327 (34088). Elemental analysis calc. $C_{20}H_{15}N_5$: C, 73.8; H, 4.65; N, 21.5. Found: C, 73.3; H, 4.75; N, 21.6%. X-ray structure analysis: $C_{20}H_{15}N_5{\cdot}CH_3OH$, M = 357.41 g mol^{-1}, CCDC 1038552.

Data for L^3. Yield: 0.39 g, 16%, white powder. Melting point: 244–246 °C. Thin layer chromatography (CH_2Cl_2/CH_3OH; 150:1): R_f ~ 0.36. ESI-TOF MS (CH_2Cl_2): m/z = 340.16 M+H^+. ^{1}H NMR (500 MHz, DMSO-d_6, 25 °C) δ(ppm) 12.75 (s, 1H), 8.44 (dd, J = 8, 1H), 8.32 (dd, J = 7.5 Hz, 1H), 8.19 (t, J = 7.75, 1H), 7.77 (t, J = 8.25, 2H), 7.69 (s, 2H), 7.36 (t, J = 7.5, 1H), 7.31–7.26 (m, 3H), 5.01 (q, J = 7.25 Hz, 2H), 1.27 (s, J = 7.25 3H). ^{13}C NMR (125 MHz, DMSO-d_6, 25 °C) δ(ppm) 150.20, 150.01, 149.04, 148.17, 142.25, 138.72, 135.96, 125.25, 123.33, 122.41, 122.15, 119.66, 110.86, 15.32. FT-IR (KBr): ν/cm^{-1} = 3457, 3051, 2977, 2933, 1593(m), 1571(m), 1467, 1443(s), 1424, 1380, 1354, 1331, 1314, 1274, 1258, 1229, 1196, 1153, 1133, 1111, 1074, 1005, 976, 861, 824(m), 742(s), 714, 658, 618, 583, 564, 522, 461, 427. UV/VIS (CH_2Cl_2): λ_{max} (ε, M^{-1} cm^{-1}) = 328 (33522). Elemental analysis calc. $C_{21}H_{17}N_5$: C, 74.3; H, 5.05; N, 20.6. Found: C, 73.1; H, 4.93; N 20.4%. X-ray structure analysis: $C_{21}H_{17}N_5{\cdot}(CH_3)_2SO{\cdot}H_2O$, M = 435.54 g mol^{-1}, CCDC 1038554.

Data for L^4. Yield: 0.29 g, 11%, white powder. Melting point: 208–210 °C. Thin layer chromatography (CH_2Cl_2/CH_3OH; 150:1): R_f ~0.33. ESI-TOF MS (CH_2Cl_2): m/z = 354.17 M+H^+. ^{1}H NMR (500 MHz, DMSO-d_6, 25 °C) δ(ppm) 12.71 (s, 1H), 8.44 (dd, J = 8 Hz, 1H), 8.20 (t, J = 7.75 Hz, 1H), 8.08 (dd, J = 7.5, 1H), 7.88 (d, J = 7.5, 1H), 7.75 (d, J = 8 Hz, 1H), 7.66 (s, 2H), 7.33–7.24 (m, 4H), 5.32 (sx, J = 6.75 Hz, 1H), 1.66 (d, J = 7 Hz, 6H).^{13}C NMR (125 MHz, DMSO-d_6, 25 °C) δ(ppm) 150.35, 150.31, 150.24, 148.23, 142.96, 138.69, 133.76, 126.08, 122.82, 122.15, 121.98, 119.96, 113.08, 48.87, 21.11. FT-IR (KBr): ν/cm^{-1} = 3453, 3065, 2300, 2969, 2937, 1923, 1888, 1852, 1770, 1612, 1590(m), 1571 (m), 1484, 1444(s), 1419, 1391, 1380, 1336, 1315, 1285, 1253, 1225, 1192, 1164, 1133, 1105, 1090, 1051, 1009, 993, 979, 926, 901, 856, 828(m), 766, 749, 739(s), 661, 639, 565, 535, 516, 478, 446, 423. UV/VIS (CH_2Cl_2): λ_{max} (ε, M^{-1} cm^{-1}) = 358 (21694), 308 (27786). Elemental analysis calc. $C_{22}H_{19}N_5$: C, 74.8; H, 5.42; N, 19.8. Found: C, 74.2; H 5.22; N, 19.8%. X-ray structure analysis: $C_{22}H_{19}N_5$, M = 353.42 g mol^{-1}, CCDC 1038556.

Data for L^5. Yield: 0.45 g, 12%, white powder. Melting point: 214–216 °C. Thin layer chromatography (CH_2Cl_2/CH_3OH; 150:1): R_f ~0.596. ESI-TOF MS (CH_3CN): m/z = 514.30 M+H^+. ^{1}H NMR (500 MHz, DMSO-d_6, 25 °C) δ(ppm) 12.83 (s, 1H), 8.40 (d, J = 7.5, 1H), 8.24 (d, J = 8 Hz, 1H), 8.14 (t, J = 7.75, 1H), 8.02 (d, J = 8, 1H), 7.68 (s, 2H), 7.40 (t, J = 7.75 Hz, 1H), 7.33–7.27 (m, 4H), 7.07 (s, 1H), 6.84 (s, 2H), 6.32 (s, 2H), 0.94 (s, 18H). ^{13}C NMR (125 MHz, DMSO-d_6, 25 °C) δ(ppm) 150.25, 150.13, 150.02, 149.22, 148.03, 142.15, 138.66, 136.91, 136.72, 125.12, 123.52, 122.59, 121.92, 121.21, 120.64, 119.72, 111.28, 48.19, 34.08, 30.80. FT-IR (KBr): ν/cm^{-1} = 3676, 3629, 3376, 3053, 2963(s), 2904, 2867, 2520, 1981, 1931, 1901, 1770, 1670, 1597(s), 1573(s), 1515, 1461, 1447 (s), 1405, 1395, 1385, 1363, 1346, 1330, 1316, 1290, 1278, 1249 (m), 1231, 1201, 1164, 1153, 1117, 1096, 1075, 1037, 1009, 994, 971, 928, 890, 879, 863, 823(s), 803, 763, 745(s), 714, 658, 618, 593, 580, 566, 545, 523, 457, 427, 397. UV/VIS (CH_2Cl_2): λ_{max} (ε, M^{-1} cm^{-1}) = 326 (43750). Elemental analysis calc. $C_{34}H_{35}N_5$: C, 79.5; H, 6.87; N, 13.6. Found: C, 79.6; H, 6.73; N, 13.1%. X-ray structure analysis: $C_{34}H_{35}N_5{\cdot}(CH_3)_2SO{\cdot}H_2O$, M = 609.81 g mol^{-1}, CCDC 1038557.

Data for L^6. The crude product was recrystallized from toluene (2 × 10 cm^3). Yield: 0.49 g, 14%, white powder. Melting point: 276–278 °C. Thin layer chromatography (CH_2Cl_2/CH_3OH; 150:1): R_f ~0.451. ESI-TOF MS (CH_2Cl_2/CH_3OH): m/z = 482.08 M+H^+. ^{1}H NMR (500 MHz, DMSO-d_6, 25 °C) δ(ppm) 12.61 (s, 1H), 8.40 (dd, J = 10 Hz, 1H), 8.30 (dd, J = 7.5 Hz, 1H), 8.15 (t, J = 7.75, 1H), 7.83 (q, J = 7.75, 2H), 7.69 (s, 2H), 7.38–7.24 (m, 6H), 6.93 (d, J = 8.5, 2H), 6.34 (s, 2H). ^{13}C NMR (125 MHz, DMSO-d_6, 25 °C) δ(ppm) 149.99, 149.71, 149.17, 147.93, 142.18, 138.83, 137.27, 136.58, 131.58, 131.45, 128.63, 125.19, 123.77, 122.79, 122.18, 120.32, 119.82, 111.20, 47.38. FT-IR (KBr): ν/cm^{-1} = 3397(s), 3060, 2917, 2849, 1598, 1574, 1488, 1458(s), 1436(m), 1418(m), 1354, 1329, 1314, 1277, 1253, 1234, 1218, 1169, 1156, 1068, 1010, 994, 969, 895, 859, 822, 807, 797, 765, 752, 745(s), 659, 586, 576, 568, 556, 476, 457, 429. Elemental analysis calc. $C_{26}H_{18}N_5Br$: C, 65.0; H, 3.78; N, 14.7. Found: C, 65.0; H, 3.83; N, 14.1%.

2.5. Synthesis of Fe(II) complexes $[Fe(L^n)_2](ClO_4)_2$

Mononuclear Fe(II) complexes containing ligands L^2 through L^5 have been synthesized by the following general recipe. A 100 cm^3 two necked round-bottomed flask was charged with ligand L^n (0.31 mmol) dissolved in methanol (50 cm^3) and/or acetonitrile for L^5. Argon was passed through the solution for 30 min. to remove dissolved air and then $Fe(ClO_4)_2$ hexahydrate (0.039 g, 0.15 mmol) was added once. The mixture was stirred at 65–70 °C overnight with colour changing to violet-pink. Single crystals were grown by using ACN/Et_2O.

Data for $[Fe(L^2)_2](ClO_4)_2$ (**2**). Yield: 0.12 g, 86%. Melting point 284–286 °C. ESI-TOF MS (CH_2Cl_2): m/z = 353.09 M^{2+}. UV/VIS (Nujol): $\nu_{max}/10^3$ cm^{-1} (relat. absorb.) = 27.100 (0.926), 19.763 (0.615), 18.149 (0.639), 14.085 (0.319). UV/VIS (CH_2Cl_2): λ_{max} (ε, M^{-1} cm^{-1}) = 321 (57962), 369 (47770), 574 (6688). FT-IR (KBr): ν/cm^{-1} = 3408, 3060, 1608, 1573, 1519, 1489, 1469(s), 1423, 1349, 1324(m), 1261, 1231, 1109(s), 1089(s), 1019, 930, 911, 858, 805, 744(s), 674, 626(m), 430. Elemental analysis calc. $C_{40}H_{30}Cl_2N_{10}FeO_8$: C, 53.1; H, 3.34; N, 15.5. Found: C, 53.0; H, 3.71; N, 15.9%.

Data for $[Fe(L^3)_2](ClO_4)_2$ (**3**). Yield: 0.11 g, 80%. Melting point 268-270 °C. ESI-TOF MS (CH_2Cl_2): m/z = 367.12 M^{2+}. UV/VIS (Nujol): $\nu_{max}/10^3$ cm^{-1} (relat.absorb.) = 27.027 (0.913), 19.960 (0.574), 18.149 (0.601), 14.184 (0.300). UV/VIS (CH_2Cl_2): λ_{max} (ε, M^{-1} cm^{-1}) = 321 (56481), 369 (48765), 574 (6481). FT-IR (KBr): ν/cm^{-1} = 3446, 3065, 2975, 1607, 1573, 1512, 1461(s), 1385, 1323, 1232, 1190, 1101(s), 928, 866, 814, 744(s), 622(m), 430, 380. Elemental analysis calc. $C_{42}H_{34}Cl_2FeN_{10}O_8$: C, 54.0; H, 3.67; N, 15.0. Found: C, 54.6; H, 4.00; N, 15.3%.

Data for $[Fe(L^4)_2](ClO_4)_2$ (**4**). Yield: 0.14 g, 79%. Melting point 204-206 °C. ESI-TOF MS (CH_2Cl_2): m/z = 381.13 M^{2+}. UV/VIS (Nujol): $\nu_{max}/10^3$ cm^{-1} (relat absorb.) = 27.027 (0.762), 19.802 (0.460), 17.637 (0.492), 14.184 (0.219). UV/VIS (CH_2Cl_2): λ_{max} (ε, M^{-1} cm^{-1}) = 321 (60943), 370 (43098), 573 (6061). FT-IR (KBr): ν/cm^{-1} = 3448, 3066, 2979, 1606, 1573, 1499, 1479, 1455(s), 1375, 1335, 1323, 1290, 1258, 1232, 1218, 1105(s), 1018, 929, 865, 822, 801, 764, 743(s), 675, 656, 623(m), 561, 431. Elemental analysis calc. $C_{44}H_{38}Cl_2FeN_{10}O_8$: C, 54.96; H, 3.98; N, 15.7. Found: C, 55.1; H, 4.01; N, 15.7%.

Data for $[Fe(L^5)_2](ClO_4)_2$ (**5**). Used reagents: L^5 (0.251 g, 0.49 mmol) dissolved in acetonitrile (80 cm^3); iron(II) perchlorate hexahydrate (0.062 g, 0.25 mmol. Yield: 0.25 g, 80%. Melting point 252-254 °C. ESI-TOF MS (CH_2Cl_2): m/z = 541.26 M^{2+}. UV/VIS (Nujol): $\nu_{max}/10^3$ cm^{-1} (relat. absorb.) = 26.954 (0.586), 17.452 (0.347), 14.184 (0.102). UV/VIS (CH_2Cl_2): λ_{max} (ε, M^{-1} cm^{-1}) = 321 (60738), 370 (49329), 573 (7047). FT-IR (KBr): ν/cm^{-1} = 3370, 3187, 3068, 2962(s), 2905, 2867, 1777, 1662(w), 1602(m), 1573, 1510, 1465(s), 1444, 1395, 1364, 1325, 1276, 1233, 1200, 1102(s), 1020, 1011, 927, 899, 868, 823, 808, 762, 745(s), 712, 675660, 623(s), 565, 431. Elemental analysis calc. $C_{68}H_{70}Cl_2N_{10}FeO_8$: C, 63.7; H, 5.50; N, 10.9. Found: C, 63.4; H, 5.77; N, 11.2%.

2.6. Synthesis of Fe(II) complexes with deprotonated ligands

Iron(II) complexes with monodeprotonated ligands L^2_{1H} through L^5_{1H} were prepared as follows. In a 100 cm^3 two necked round-bottomed flask a crude solid complex $[Fe(L^n)_2](ClO_4)_2$ was dissolved in dichloromethane (50 cm^3) under argon atmosphere. After 30 min. of stirring, a solid Na_2CO_3 was added and the mixture stirred at 39 °C for overnight resulting in a blue colour.

Data for $[Fe(L^2_{1H})_2]$ (**2d**). Used reagents: $[Fe(L^2)_2](ClO_4)_2$ (0.051 g, 0.06 mmol); Na_2CO_3 (0.024 g, 0.23 mmol, 4 eq.). Yield: 0.04 g, 95%. Melting point 225–227 °C. ESI-TOF MS (CH_2Cl_2): m/z = 705.19 M +H^+. FT-IR (KBr): ν/cm^{-1} = 3360, 3055, 2964, 1604, 1571, 1501, 1487, 1452, 1433, 1415, 1326, 1262(s), 1228, 1095(s), 1023(s), 863, 803(s), 741(s), 622, 428. UV/VIS (Nujol): $\nu_{max}/10^3$ cm^{-1} (relat. absorb.) = 30.488 (0.809), 27.397 (0.560), 16.835 (0.393), 12.391 (0.184). UV/VIS (CH_2Cl_2/CH_3OH; 5:1): λ_{max} (ε, M^{-1} cm^{-1}) = 322 (39942), 368 (25073), 578 (3499). Elemental analysis calc. $C_{40}H_{28}FeN_{10}$: C, 68.2; H, 4.01; N, 19.9. Found: C, 68.4; H, 4.44; N 19.7%. X-ray structure analysis: $C_{40}H_{28}FeN_{10}{\cdot}(CH_3CH_2)_2O{\cdot}CH_3OH$, M = 810.74 g mol^{-1}, CCDC 1038553.

Data for $[Fe(L^3_{1H})_2]$ (**3d**). Used reagents: $[Fe(L^3)_2](ClO_4)_2$ (0.090 g, 0.10 mmol); Na_2CO_3 (0.041 g, 0.39 mmol, 4 eq.). Yield: 0.07 g, 92%. Melting point 210–212 °C. There is a continuous mass loss of 7% until 210 °C accompanied by an exothermic peak. ESI-TOF MS (CH_2Cl_2): m/z = 733.22 M+H^+. FT-IR (KBr): ν/cm^{-1} = 3392, 3055, 2964, 1631, 1603, 1573, 1434(s), 1381, 1349, 1327, 1092(s), 1019, 868, 803(s), 742, 627, 429. UV/VIS (Nujol): $\nu_{max}/10^3$ cm^{-1} (relat. absorb.) = 26.882 (0.722), 16.695 (0.523), 12.3916 (0.271). UV/VIS (CH_2Cl_2/CH_3OH; 5:1): λ_{max} (ε, M^{-1} cm^{-1}) = 307 (39934), 347 (38944), 598 (5281). Elemental analysis calc. $C_{42}H_{32}FeN_{10}$: C, 69.8; H, 4.26; N, 18.5. Found: C, 69.4; H, 4.35; N, 18.9%. X-ray structure analysis: $C_{42}H_{32}FeN_{10}{\cdot}3CH_3CN$, M = 855.79 g mol^{-1}, CCDC 1038555.

Data for $[Fe(L^4_{1H})_2]$ (**4d**). Used reagents: $[Fe(L^4)_2](ClO_4)_2$ (0.080 g, 0.08 mmol); Na_2CO_3 (0.035 g, 0.33 mmol, 4 eq.). Yield: 0.06 g, 87%. Melting point 160–162 °C. There is a continuous mass loss of 5% until 210 °C accompanied by a broad exothermic peak at 160 °C, then a sharp exothermic peak at 180 °C, and a sharp endothermic peak at 200 °C. ESI-TOF MS (CH_2Cl_2): m/z = 760.25 M A79. UV/VIS (Nujol): $\nu_{max}/10^3$ cm^{-1} (relat. absorb.) = 26.954 (0.841), 16.863 (0.504), 14.025 (0.254). UV/VIS (CH_2Cl_2/CH_3OH; 5:1): λ_{max} (ε, M^{-1} cm^{-1}) = 323 (52339), 369 (16959), 579 (1754) A80. FT-IR (KBr): ν/cm^{-1} = 3057, 2929, 2857, 1739, 1664, 1595, 1572, 1448(s), 1388, 1326, 1315, 1289, 1256, 1229, 1191, 1159, 1133, 1100(s), 1009, 993, 930, 912, 854, 824, 808, 767, 745(s), 656, 623, 565, 533, 428, 386. Elemental analysis calc. $C_{44}H_{36}FeN_{10}$: C, 69.5; H, 4.77; N, 18.4. Found: C, 69.0; H, 4.34; N, 18.2%.

Data for $[Fe(L^5_{1H})_2]$ (**5d**). Used reagents: $[Fe(L^5)_2](ClO_4)_2$ (0.312 g, 0.24 mmol); Na_2CO_3 (0.103 g, 0.97 mmol, 4 eq.). Yield: 0.26 g, 97%. Melting point 220–222 °C. There is a continuous mass loss of 4% until 220 °C accompanied by an exothermic peak; another exothermic peak appears at 280 °C. ESI-TOF MS (CH_2Cl_2): m/z = 1081.51 M+H^+ A81.UV/VIS (Nujol): $\nu_{max}/10^3$ cm^{-1} (relat. absorb.) = 27.548 (1.242), 16.260 (0.721), 13.298 (0.315), 12.107 (0.279). UV/VIS (CH_2Cl_2/CH_3OH; 5:1): λ_{max} (ε, M^{-1} cm^{-1}) = 308 (48860), 356 (40717), 580 (3909) A82. FT-IR (KBr): ν/cm^{-1} = 3375, 3058, 2962, 2903, 2867, 1602, 1572, 1543, 1476, 1435(s), 1394, 1394, 1363, 1325, 1278, 1249, 1198, 1155, 1092(s), 1016, 979, 927, 899, 867, 850, 823, 803, 741(s), 711, 673, 659, 622, 594, 433. Elemental analysis calc. $C_{68}H_{68}FeN_{10}$: C, 75.5; H, 6.34; N, 13.0. Found: C, 75.3; H, 6.28; N, 13.5%.

2.7. X-ray structure determination

Single-crystal X-ray diffraction experiments and data collection for ligands L1 through L6 were conducted using Xcalibur S CCD (Oxford Diffraction) at 293 K. Intensities were recorded with a ω scans. Corrections for Lorentz, polarization and multi-scan absorption effects were applied. Diffraction data of **2d** and **3d** were collected on STOE IPDS II or STOE IPDS 2T diffractometers at low temperature. Graphite-monochromated Mo Kα radiation, λ = 0.71093 Å, was used. The structures were either solved by charge-flipping or direct methods and subsequent Fourier differences techniques. Non-hydrogen atoms were refined anisotropically against F^2 by common least-squares methods. The programs SUPERFLIP, SHELX (ver. 2014/7), OLEX2 and MERCURY have been used for structure determination, refinement and drawing [21–26]. The hydrogen atoms were refined with fixed distances from the parent carbon atoms.

2.8. Magnetic data collection

The magnetic measurements were conducted using a SQUID apparatus (MPMS-XL7, Quantum Design) in the RSO mode of detection. The polycrystalline sample was encapsulated in a diamagnetic gelatine-made sample holder. The susceptibility taken at $B = 0.1$ or 0.5 T has been corrected for the underlying diamagnetism and transformed to the effective magnetic moment calculated as $\mu_{eff}/\mu_B = 798(\chi' T)^{1/2}$ (SI units). For high-temperature range above 300 K an oven has been installed. Due to a different sample holder the analyzed data does not necessarily follow the 300 K tail and some discontinuity is registered.

3. Results and discussion

3.1. Organic synthesis

The 2,6-bis(2-benzimidazolyl)pyridine, as the bearer of N-donors atoms, was synthesized many times by the Phillips condensation reaction [27,28]. One of the easiest ways to attach a new substituent to the skeleton of this ligand leads by N-alkylation of benzimidazole rings. The Williams synthetic route has looked as the promising for the preparation of unsymmetrical *bzimpy* ligands extended on the benzimidazole rings [29,30]. The ratio of reactants, ligand: base: alkyl halides, was selected to minimize the effect of dialkylation. Five novel ligands L^2–L^6 were synthesized. Four of them (L^1–L^5) were used to coordination with iron salts. Due to the worse solubility of L^6 (toluene), it has not been to try yet.

Table 1
Crystal data for Fe(II) complexes with deprotonated ligands.

Abbr.	**2d**	**3d**
Empirical formula	$C_{45}H_{42}FeN_{10}O_2$	$C_{48}H_{41}FeN_{13}$
Formula weight (g mol^{-1})	810.74	855.79
Crystal system	monoclinic	monoclinic
Space group	*C*2/*c*	*C*2/*c*
T (K)	150(2)	180(2)
Crystal size (mm)	0.23 × 0.03 × 0.02	0.32 × 0.30 × 0.26
Z	4	4
a (Å)	14.4272(12)	15.4016(6)
b (Å)	15.3787(8)	16.2551(8)
c (Å)	17.9306(14)	16.7971(7)
α (°)	90	90
β (°)	106.845(6)	101.431(3)
γ (°)	90	90
V (Å^3)	3807.6(5)	4121.8(3)
D_{calc} (g cm^{-3})	1.414	1.379
Absorption coefficient (mm^{-1})	0.451	0.419
Reflections collected/unique	10073/4021	11353/3871
Data/restraints/parameters	4021/0/275	3871/0/264
Goodness-of-fit (GOF) on F^2	1.008	1.043
Final *R* indices ($I > 2\sigma(I)$)	$R_1 = 0.0944$ $wR_2 = 0.2056$	$R_1 = 0.0667$ $wR_2 = 0.1771$
R indices (all data)	$R_1 = 0.1349$ $wR_2 = 0.2235$	$R_1 = 0.0815$ $wR_2 = 0.1865$
Largest difference peak and hole (e Å^{-3})	2.415/−0.732	1.377/−0.761
CCDC No.	1038553	1038555

3.2. Molecular and crystal structure

Crystal data, information about data collection and structure analysis for ligands L^1 through L^6 were forwarded to Electronic Supplementary Information (ESI). The data referring to the Fe(II) complexes with deprotonated ligands, **2d** and **3d**, are listed in Table 1.

The structure of the compound **2d**·is formed by molecular units ($Z = 4$) and solvent molecules of diethyl ether and methanol which are present in the crystal lattice. The Fe(II) centre is hexacoordinate with two deprotonated ligands in the coordination environment (Fig. 1). The bond lengths of Fe–N(pyridine) equals to 1.900 Å and those of Fe–N(imidazole) are 1.972 and 1.939 Å, respectively (Table 2). This indicates the low-spin state of the complex at 150 K. Two benzene rings belonging to the neighbouring molecular units, show a perfect π–π stacking at the C···C contact of 3.67 Å.

The molecular and crystal structure of **3d** is essentially analogous to **2d** (Fig. 2). The shortest bond lengths Fe–N(pyridine) within the chromophore equal to 1.906 Å and those of Fe–N(imidazole) are 1.965 and 1.976 Å, respectively. Centroid-centroid distances between the stacked benziimidazole rings are 3.675 Å for **2d** and 3.724 for **3d**.

The analogous Fe(II) complex with the deprotonated ligand *bzimpy*$_{-1H}$ (abbr. **1d**) possesses the distances of Fe-N(pyridine) = 1.918 Å and Fe–N(imidazole) = 1.950 Å, respectively [17]; the molecular and crystal structure of **1d**·H_2O is viewed in Fig. 3.

3.3. Spectral data and electronic structure

Electronic spectra for complexes containing protonated *bzimpy* ligands (**2**–**5**), as well as, for complexes containing deprotonated ligands (**2d**–**5d**) have been measured in solid state (nujoll mull) and are shown in Fig. S43 in ESI. One can easily recognize the almost identical spectral profile for all compounds, that is characterized by a small peak at ~17 180 cm^{-1} followed by a more intense peaks located at ~27 400 and 31 900 cm^{-1}.

To elucidate the electronic structure of complexes under study and also the origin of the spectral transitions, we have calculated electronic spectra for three complexes **1d**, **2d** and **3d** containing deprotonated *bzimpy* derivatives [31]. To carry out this objective, the time-dependent restricted Kohn-Sham formalism has been chosen, due to the proven low-spin ($S = 0$) ground state of the **1d**. According to the structural similarities of **1d** with **2d** and **3d**, we suspect to such magnetic behaviour also in the later two

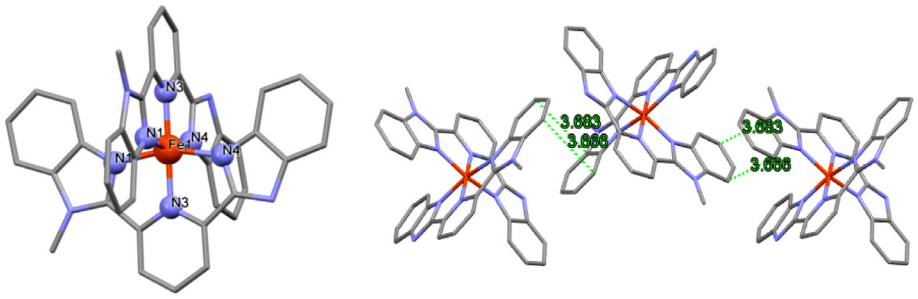

Fig. 1. The structure of Fe(II) complexes **2d** with deprotonated ligands at 150 K. Hydrogen atoms and crystal solvent molecules are omitted for clarity. Left – molecular structure, right – the π–π stacking between benzene rings.

Table 2
Bond lengths (Å) within the chromophore of **2d** and **3d**.

2d	T = 150 K	**3d**	T = 180 K
Fe(1)–N(1)	1.972(4)	Fe(1)–N(3)	1.906(3)
Fe(1)–N(1)$^{\#1}$	1.972(4)	Fe(1)–N(3)$^{\#1}$	1.906(3)
Fe(1)–N(3)	1.900(3)	Fe(1)–N(4)	1.965(3)
Fe(1)–N(3)$^{\#1}$	1.900(3)	Fe(1)–N(4)$^{\#1}$	1.965(3)
Fe(1)–N(4)	1.939(4)	Fe(1)–N(2)	1.976(3)
Fe(1)–N(4)$^{\#1}$	1.939(4)	Fe(1)–N(2)$^{\#1}$	1.976(3)

complexes. Calculations have been performed on X-ray structure coordinates employing hybrid B3LYP functional and def2-TZVP basis set [32–34].

The main results are compiled in Figs. 4 and 5. From these, we can see that the calculated electronic spectra are in good agreement with the experimental ones. Furthermore, we can recognize similarities in electronic structure, especially for complexes **2d** and **3d**. Complex **1d** shows slight differences. Due to the complex nature of the excited states, we have analyzed the principal electronic transitions in terms of difference densities. This approach has helped us to recover the simple single-electron picture of the transitions that is depicted in Fig. S44 (for **1d**) and Fig. S45 (for **3d**) in ESI. For complex **2d** the excitations are identical with those of **3d**. As can be seen (Fig. 4), in **1d** the transitions under 20 000 cm^{-1} can be characterized as ligand-to-metal charge transfer (LMCT) due to mainly ligand character of the highest occupied orbitals. At higher energies (>20 000 cm^{-1}) the electron relocations to π-character metal–ligand orbitals can be identified. In case of **2d** and **3d** the metal-to-ligand charge transfers (MLCT) are dominated with relocations to pyridyl moiety of the *bzimpy*$_{\text{-1H}}$ ligands.

Effect of the ligand substituents on electronic structure has been studied on free ligands (L^1–L^5 and L^1_{1H}–L^5_{1H} X-ray structures).

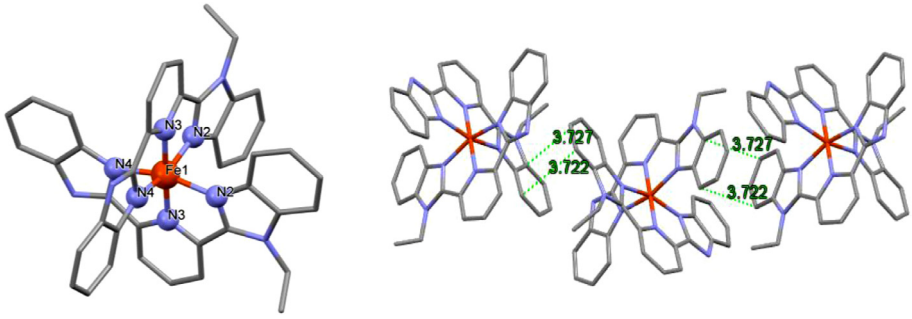

Fig. 2. The structure of Fe(II) complexes **3d** with deprotonated ligands at 180 K. Hydrogen atoms and crystal solvent molecules are omitted for clarity. Left – molecular structure, right – the π-π stacking between benzene rings.

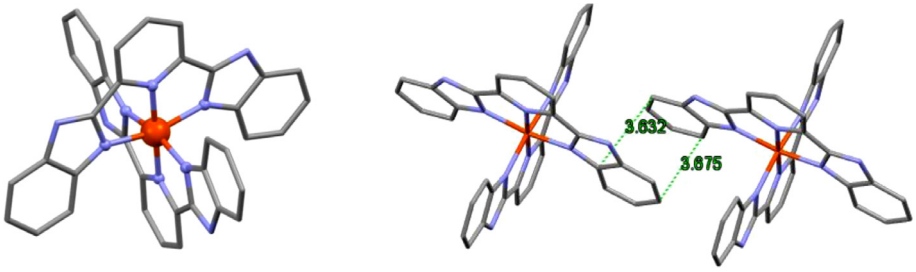

Fig. 3. The structure of Fe(II) complexes **1d**·H_2O with deprotonated ligands at 293 K [9]. Hydrogen atoms and crystal solvent molecules are omitted for clarity. Left – molecular structure, right – the π–π stacking between benzene rings.

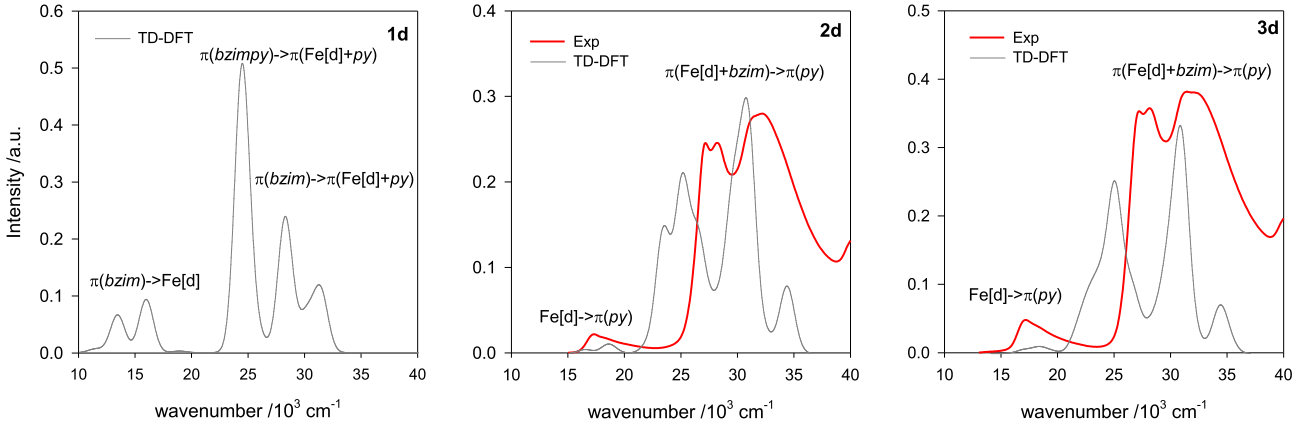

Fig. 4. Comparison of measured and calculated electronic spectra of complexes **1d**, **2d** and **3d** (*bzim* = benzimidazolyl moiety of the *bzimpy*$_{\text{-1H}}$ ligands, *py* = pyridyl moiety of the *bzimpy*$_{\text{-1H}}$ ligands). Calculated intensities were divided by a factor 3 × 10^5.

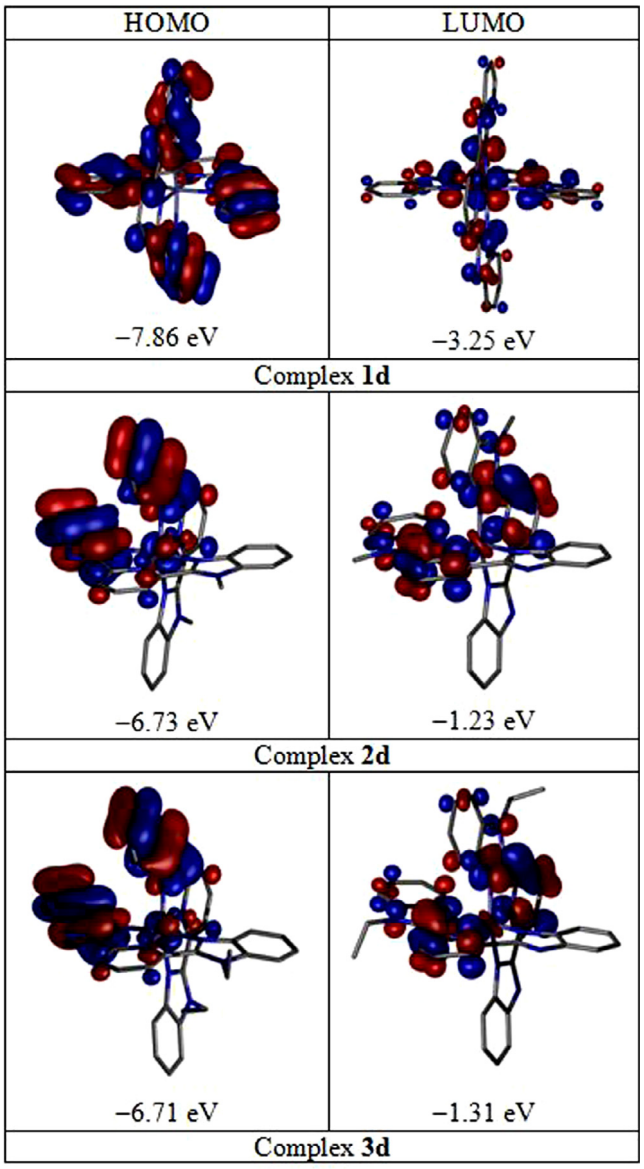

Fig. 5. Frontier orbitals of **1d**, **2d** and **3d**.

Natural population analysis (B3LYP/6-311G*) has been performed to obtain natural charges on nitrogen donor atom [35]. Results are shown in Fig. 6 (see also Figs. S46–S50 in ESI). According to these findings, deprotonation of the benzimidazolyl subunits increases electron density on nitrogen donors of the benzimidazolyls and decreases electron density on the pyridyl nitrogen. Introduction of methyl substituent on the benzimidazolyl and further extension of the alkyl chain affect the electronic structure slightly (moderate variation of the negative charge from L^1 to L^5). Significantly greater impact brings the deprotonation of the ligands. Recently studies have shown that the low-spin state of such complexes is stabilized by electron-withdrawing pyridyl substituents, but also by electron-donating substituents located on the peripheral ligand subunits (such as a benzimidazolyl) [36,37]. Alkyls and phenyls are weakly electron-donating groups, thus the low-spin is stabilized in complexes under study.

3.4. Magnetic data

Magnetic data for $[Fe(L^2)_2](ClO_4)_2$ (**2**) is shown in Fig. 5. At $T = 1.9$ K the effective magnetic moment adopts a value of $\mu_{eff} = 0.58\ \mu_B$. On heating it shows only a small increase to $\mu_{eff} = 1.57\ \mu_B$ at the room temperature. Such a behaviour is characteristic for the $S = 0$ state with some temperature-independent paramagnetism (TIP; it appears as an effect of the presence of close-lain excited states). It is confirmed that **2** is a low-spin Fe (II) complex until $T = 300$ K.

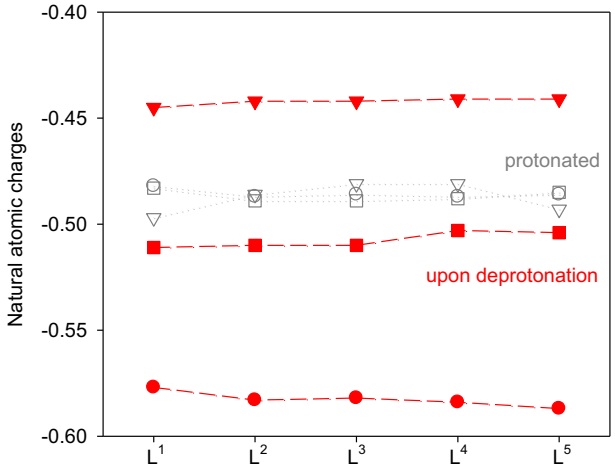

Fig. 6. Calculated natural atomic charges on nitrogen donor atoms (▼-on pyridyl moiety; ●, ■-on benzimidazolyl moieties) of free *bzimpy* ligands.

Magnetic data for the complex $[Fe(L^2_{1H})_2]$ (**2d**) is also displayed in Fig. 5. At $T = 1.9$ K the value of $\mu_{eff} = 0.91\ \mu_B$ reflects the $S = 0$ state with some paramagnetic impurity (as confirmed by the magnetic susceptibility). On heating the effective magnetic moment slowly increases until $T \approx 47$ K and the increase continues up to the ambient temperature where $\mu_{eff} = 1.45\ \mu_B$. High-temperature measurements (with the installed "owen") were conducted in the cooling mode $T = 551$–300 K as well as in the heating direction $T = 301$–501 K. These data superimpose and at the end of the heating ($T = 501$ K) $\mu_{eff} = 2.07\ \mu_B$. Above $T > 500$ K an on-set of the spin transition is indicated based upon a more rapid increase of the effective magnetic moment.

Fig. 6 brings the magnetic data for the complex $[Fe(L^3)_2](ClO_4)_2$ (**3**). At $T = 1.9$ K the effective magnetic moment is only $\mu_{eff} = 0.52\ \mu_B$ and on heating it increases gradually to $\mu_{eff} = 1.25\ \mu_B$ at $T = 300$ K. Again the diamagnetic ($S = 0$) state is confirmed until room temperature.

Magnetic data for $[Fe(L^3_{1H})_2]$ (**3d**) is also shown in Fig. 6. At $T = 1.9$ K the value of $\mu_{eff} = 0.92\ \mu_B$ and this system behaves analogously to the previous case so that **3** is low-spin ($S = 0$) until $T = 300$ K. High-temperature measurements (with the installed "owen") in the heating mode $T = 354$–552 K and in the cooling mode $T = 547$–469 K, however, are different. On heating the effective magnetic moment slowly increases from $\mu_{eff} = 0.62\ \mu_B$ at $T = 354$ K to $\mu_{eff} = 1.38\ \mu_B$ at $T = 552$ K. On cooling the effective magnetic moment stays almost constant between $\mu_{eff} = 1.39\ \mu_B$ at $T = 546$ K and $\mu_{eff} = 1.36\ \mu_B$ at $T = 469$ K.

Magnetic data for $[Fe(L^4)_2](ClO_4)_2$ (**4**) is shown in Fig. 7 and it is essentially similar to that for **3** and **2**. To this end, **4** is a low-spin Fe (II) complex until $T = 300$ K. For $[Fe(L^4_{1H})_2]$ (**4d**) at $T = 1.9$ K the value of $\mu_{eff} = 0.37\ \mu_B$ and on heating it slightly increases to $\mu_{eff} = 1.50\ \mu_B$ at $T = 300$ K also confirming the diamagnetic state, $S = 0$.

Fig. 8 brings magnetic data for $[Fe(L^4)_2](ClO_4)_2$ (**5**). At $T = 1.9$ K the effective magnetic moment is only $\mu_{eff} = 0.55\ \mu_B$; on heating it increases to $\mu_{eff} = 1.83\ \mu_B$ at the room temperature. These data match the diamagnetic state ($S = 0$) until ambient temperature. Magnetic data for $[Fe(L^5_{1H})_2]$ (**5**) is also shown in Fig. 8. The sample

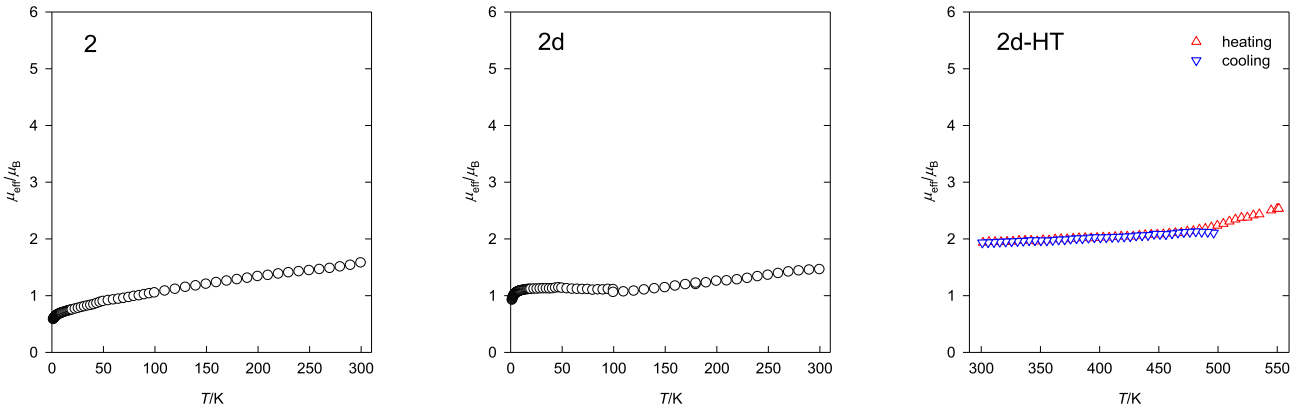

Fig. 7. Magnetic data for $[Fe(L^2)_2](ClO_4)_2$ and $[Fe(L^2_{-1H})_2]$ complexes.

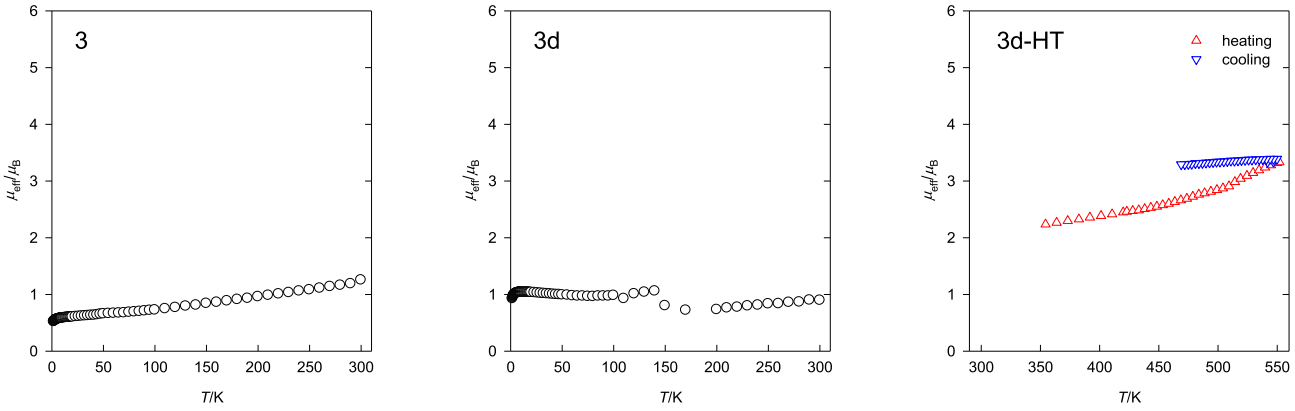

Fig. 8. Magnetic data for $[Fe(L^3)_2](ClO_4)_2$ and $[Fe(L^3_{-1H})_2]$ complexes.

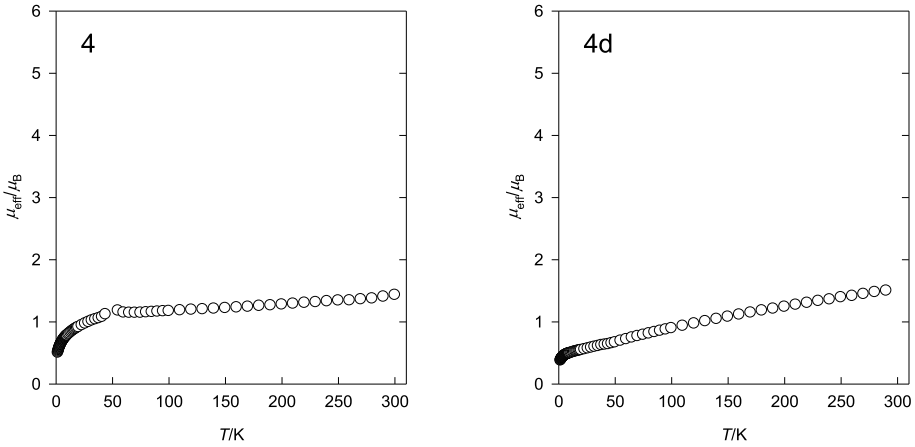

Fig. 9. Magnetic data for $[Fe(L^4)_2](ClO_4)_2$ and $[Fe(L^4_{-1H})_2]$ complexes.

Table 3
Comparison of magnetic behaviour with literature data.

Compound	Behaviour	Refs.
$[Fe(L^1)_2](BPh_4)_2\ 4H_2O$	$S = 0$ to $S = 2$, $T_c = 300$ K	[15]
$[Fe(L^1)_2](BPh_4)_2$	High-spin, $S = 2$	[15]
$[Fe(L^1)_2](ClO_4)_2\ 0.25H_2O$	Low-spin until r.t. $S = 0$ to $S = 2$, $T_{1/2}\uparrow = 409$ K, $T_{1/2}\downarrow = 397$ K, $\Delta T = 12$ K	[16]
$[Fe(L^1_{-1H})_2]\ H_2O$	Low-spin until r.t. $S = 0$ to $S = 2$, $T_{1/2}\uparrow = 424$ K	[17]
$[Fe(L^1)_2]SO_4\ 2H_2O$	Low-spin until r.t.	unpublished
$[Fe(L_{tz})_2](ClO_4)_2{\cdot}2H_2O$	Low-spin until r.t. $S = 0$ to $S = 2$, $T_{1/2} = 323$ K, $\Delta T = 35$ K	[17]

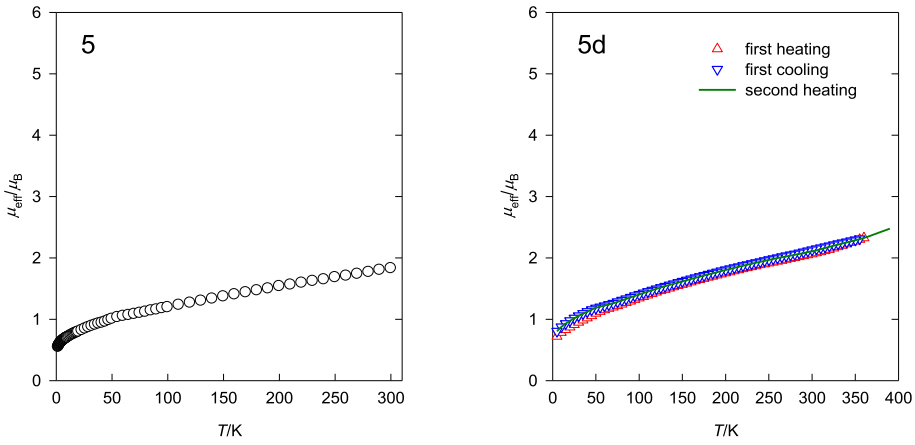

Fig. 10. Magnetic data for $[Fe(L^5)_2](ClO_4)_2$ and $[Fe(L^5_{1H})_2]$ complexes.

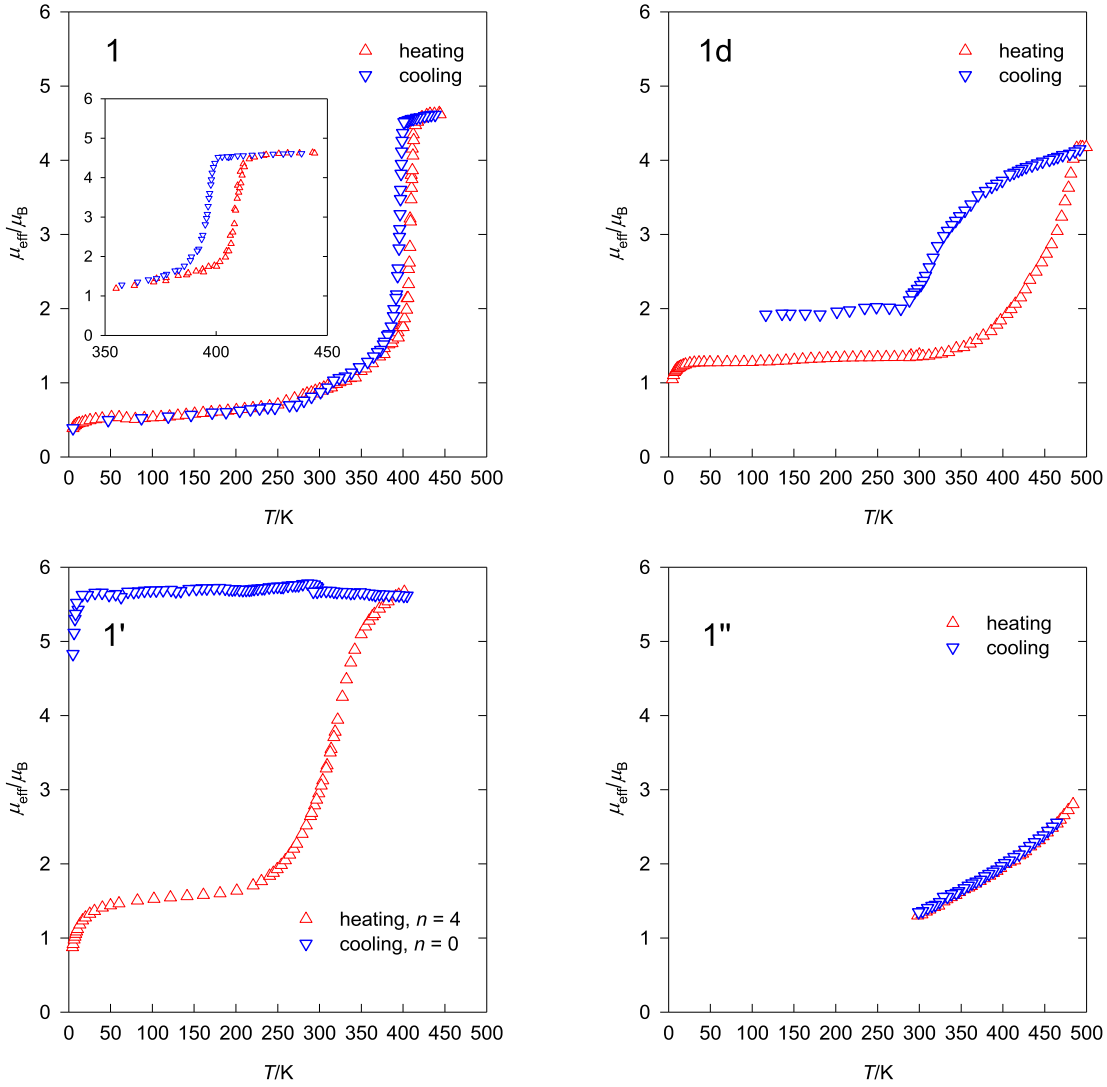

Fig. 11. Comparison of magnetic data for $[Fe(L^1)_2](ClO_4)_2{\cdot}0.25H_2O$, $[Fe(L^1_{1H})_2]{\cdot}H_2O$, $Fe(bzimpy)_2](BPh_4)_2\ nH_2O$ (**1′**) and $[Fe(bzimpy)_2](SO_4)\ 2H_2O$ (**1″**) complexes [15–17].

was cycled between 5 K and 360 K and 5 K and 390 K and 15 K. On the first heating the effective magnetic moment starts from the value of 0.72 μ_B at $T = 5$ K and increases to $\mu_{eff} = 2.32\ \mu_B$ at $T = 360$ K. On the second heating the effective magnetic moment starts from a higher value 0.80 μ_B at $T = 5$ K and increases to $\mu_{eff} = 2.48\ \mu_B$ at $T = 390$ K. Most likely the solvent was slowly evaporated by heating which slightly influences the measured magnetic moment of the specimen.

Some more data about the related complexes have been retrieved from literature [15–17] and the corresponding magnetic functions are redrawn in Fig. 9. and the transition temperature is listed in Table 3. A comparison of the data presented in Figs. 4–8 leads to the following findings (see Figs. 10 and 11).

1. The low-temperature magnetic data for $[Fe(L^n)_2](ClO_4)_2$ type complexes are influenced by some paramagnetic impurity (PI), probably traces of Fe(III). In such a case the effective magnetic moment on heating stays almost constant (the PI follows the Curie-Weiss law).
2. A constant slope of the μ_{eff} *versus T* function reflects a temperature-independent paramagnetism originating in the presence of the close-lying excited states (arising from the $^5T_{2g}$ crystal-field term).
3. There is no indication of the spin transition until the ambient temperature. However, above 300 K an on-set of the spin crossover is visible in **2d** and **3d**.
4. In the previously reported complex **1**, the transition temperature is $T_{1/2}\uparrow$ = 409 K and $T_{1/2}\downarrow$ = 397 K giving rise to the hysteresis width of ΔT = 12 K.
5. In **1d**, however, $T_{1/2}\uparrow$ = 424 K is rather high and probably the spin transition is incomplete until highest temperature of the data taking (500 K); also the release of the crystal water can modify the cooling path.
6. In **1′** four molecules of the crystal water are lost on the heating and the complex turns to the high-spin state that remains high-spin on the cooling.
7. An analogous liberation of the solvent molecules in **3d** causes that the cooling path is different from the heating one.
8. In the sulfato complex $[Fe(bzimpy)_2](SO_4)\,2H_2O$ (**1″**) the on-set of the spin crossover is registered.

4. Conclusions

Five derivatives of the basic *bzimpy* ligand have been prepared and fully characterized (X-*bzimpy*). These were used in synthesizing $[Fe(X\text{-}bzimpy)_2](ClO_4)_2$ complexes as well as the deprotonated analogues $[Fe(X\text{-}bzimpy_{-1H})_2]$. Magnetic studies reveal that all these systems are low-spin until room temperature with some on-set of the spin crossover above the room temperature.

Acknowledgments

Slovak grant agencies (APVV-14-0078, VEGA 1/0534/16 and VEGA 1/0534/16) and Marie Curie fellowship (contract No. PITN-GA-2009-238804) are acknowledged for the financial support. We thank the KIT-INT staff for their support during measurements and Dr. Šalitroš to help with high temperature SQUID measurements.

Appendix A. Supplementary data

CCDC 1038552, 1038554, 1038556 and 1038557 contains the supplementary crystallographic data for L^2, L^3, L^4, and L^5. CCDC 1038555 and 1038553 contains the supplementary crystallographic data for **2d** and **3d**. These data can be obtained free of charge via http://www.ccdc.cam.ac.uk/conts/retrieving.html, or from the Cambridge Crystallographic Data Centre, 12 Union Road, Cambridge CB2 1EZ, UK; fax: (+44) 1223-336-033; or e-mail: deposit@ccdc.cam.ac.uk. Supplementary data associated with this article can be found, in the online version, at http://dx.doi.org/10.1016/j.poly.2016.11.009.

References

[1] M. Haga, H. Hong, Y. Shiozawa, Y. Kawata, H. Monjushiro, T. Fukuo, R. Arakawa, Inorg. Chem. 39 (2000) 4566.
[2] S.P. Singh, K.S.V. Gupta, M. Chandrasekharam, A. Islam, L. Han, S. Yoshikawa, M. Haga, M.S. Roy, G.D. Sharma, Appl. Mater. Interfaces 5 (2013) 11623.
[3] M. Haga, T. Takasugi, A. Tomie, M. Ishizuya, T. Yamada, M.D. Hossain, M. Inoue, Dalton Trans. 10 (2003) 2069.
[4] X. Xiaoming, M. Haga, T. Matsumura-Inoue, Y. Ru, A.W. Addison, K. Kanod, J. Chem. Soc. Dalton Trans. 16 (1993) 2477.
[5] M. Boča, R.F. Jameson, W. Linert, Coord. Chem. Rev. 255 (2011) 290.
[6] E. Sinn, Inorg. Chim. Acta 3 (1969) 11.
[7] C.M. Harris, S. Kokot, H.R.H. Patil, E. Sinn, H. Wong, Aust. J. Chem. 25 (1972) 1631.
[8] A.M. Greenaway, E. Sinn, J. Am. Chem. Soc. 100 (1978) 8080.
[9] A.M. Greenaway, A. Schrock, E. Sinn, Inorg. Chem. 18 (1979) 2692.
[10] R.N. Grimes, R.B. Maynard, E. Sinn, G.A. Brewer, G.J. Long, J. Am. Chem. Soc. 104 (1982) 5987.
[11] A.W. Addison, S. Burman, C.G. Wahlgren, O.A. Rajan, T.M. Rowe, E. Sinn, J. Chem. Soc., Dalton Trans. (1987) 2621.
[12] D. Collison, C.D. Garner, C.M. McGrath, J.F.W. Mosselmans, M.D. Roper, J.M.W. Seddon, E. Sinn, N.A. Young, J. Chem. Soc., Dalton Trans. (1997) 4371.
[13] E.J. MacLean, C.M. McGrath, C.J. O'Connor, C. Sangregorio, J.W.M. Seddon, E. Sinn, F.E. Sowery, S.J. Teat, G.B.M. Vaughan, N.A. Young, Chem. Eur. J. 9 (2003) 5314.
[14] R. Boča, P. Baran, L. Dlháň, H. Fuess, W. Haase, F. Renz, W. Linert, I. Svoboda, R. Werner, Inorg. Chim. Acta 260 (1997) 129.
[15] R. Boča, P. Baran, M. Boča, L. Dlháň, H. Fuess, W. Haase, W. Linert, B. Papánková, R. Werner, Inorg. Chim. Acta 278 (1998) 190.
[16] R. Boča, M. Boča, Ľ. Dlháň, K. Falk, H. Fuess, W. Haase, R. Jaroščiak, B. Papánková, F. Renz, M. Vrbová, R. Werner, Inorg. Chem. 40 (2001) 3025.
[17] R. Boča, F. Renz, M. Boča, H. Fuess, W. Haase, G. Kickelbick, W. Linert, Vrbová-Schikora, Inorg. Chem. Commun. 8 (2005) 227.
[18] A.W. Addison, P.J. Burke, J. Heterocycl. Chem. 18 (1981) 803.
[19] A.W. Addison, P.J. Burke, J. Heterocycl. Chem. 20 (1983) 1481.
[20] W. Ye, M. Zhao, W. Du, Q. Jiang, K. Wu, P. Wu, Z. Yu, Chem. Eur. J. 17 (2011) 4737.
[21] L. Palatinus, G. Chapuis, J. Appl. Crystallogr. 40 (2007) 786.
[22] L. Palatinus, A. van der Lee, J. Appl. Crystallogr. 41 (2008) 975.
[23] L. Palatinus, S.J. Prathapa, S. van Smaalen, J. Appl. Crystallogr. 45 (2012) 575.
[24] G.M. Sheldrick, Acta Crystallogr. C71 (2015) 3.
[25] O.V. Dolomanov, L.J. Bourhis, R.J. Gildea, J.A.K. Howard, H. Puschmann, J. Appl. Crystallogr. 42 (2009) 339.
[26] C.F. Macrae, I.J. Bruno, J.A. Chisholm, P.R. Edgington, P. McCabe, E. Pidcock, L. Rodriquez-Monge, R. Taylor, J. van de Streek, P.A. Wood, J. Appl. Crystallogr. 41 (2008) 466.
[27] C. Piguet, J.-C.G. Bünzli, G. Bernardinelli, C.G. Bochet, P. Froidevaux, J. Chem. Soc., Dalton Trans. 4 (1995) 83.
[28] G. Muller, J.-C.G. Bünzli, K.J. Schenk, C. Piguet, G. Hopfgartner, Inorg. Chem. 40 (2001) 2642.
[29] C. Piguet, B. Bocquet, E. Müller, A.F. Williams, Helv. Chim. Acta 72 (1989) 323.
[30] C. Piguet, A.F. Williams, G. Bernardinelli, E. Moret, J.-C.G. Bünzli, Helv. Chim. Acta 75 (1992) 1697.
[31] F. Neese, The ORCA program system, Wiley Interdiscip, Rev. Comput. Mol. Sci. 2 (2012) 73.
[32] T. Petrenko, S. Kossmann, F. Neese, J. Chem. Phys. 134 (2011) 054116.
[33] F. Neese, G. Olbrich, Chem. Phys. Lett. 362 (2002) 170.
[34] T. Petrenko, O. Krylova, F. Neese, M. Sokolowski, New J. Phys. 11 (2009) 015001.
[35] M.J. Frisch, G.W. Trucks, H.B. Schlegel, G.E. Scuseria, M.A. Robb, J.R. Cheeseman, J.A. Montgomery Jr., T. Vreven, K.N. Kudin, J.C. Burant, J.M. Millam, S.S. Iyengar, J. Tomasi, V. Barone, B. Mennucci, M. Cossi, G. Scalmani, N. Rega, G.A. Petersson, H. Nakatsuji, M. Hada, M. Ehara, K. Toyota, R. Fukuda, J. Hasegawa, M. Ishida, T. Nakajima, Y. Honda, O. Kitao, H. Nakai, M. Klene, X. Li, J.E. Knox, H. P. Hratchian, J.B. Cross, V. Bakken, C. Adamo, J. Jaramillo, R. Gomperts, R.E. Stratmann, O. Yazyev, A.J. Austin, R. Cammi, C. Pomelli, J.W. Ochterski, P.Y. Ayala, K. Morokuma, G.A. Voth, P. Salvador, J.J. Dannenberg, V.G. Zakrzewski, S. Dapprich, A.D. Daniels, M.C. Strain, O. Farkas, D.K. Malick, A.D. Rabuck, K. Raghavachari, J.B. Foresman, J.V. Ortiz, Q. Cui, A.G. Baboul, S. Clifford, J. Cioslowski, B.B. Stefanov, G. Liu, A. Liashenko, P. Piskorz, I. Komaromi, R.L. Martin, D.J. Fox, T. Keith, M.A. Al-Laham, C.Y. Peng, A. Nanayakkara, M. Challacombe, P.M.W. Gill, B. Johnson, W. Chen, M.W. Wong, C. Gonzalez, J.A. Pople, Gaussian 03, Revision C.02, Gaussian Inc., Wallingford CT, 2004.
[36] M.A. Halcrow, Crystals 6 (5) (2016) 58.
[37] L.J. Kershaw Cook, R. Kulmaczewski, R. Mohammed, S. Dudley, S.A. Barrett, M. A. Little, R.J. Deeth, M.A. Halcrow, Angew. Chem., Int. Ed. 55 (2016) 4327.